Adsorption (2014) 20:311–319
DOI 10.1007/s10450-013-9586-4

Aqueous mercury adsorption in a fixed bed column of thiol functionalized mesoporous silica

Jesús M. Arsuaga · José Aguado · Amaya Arencibia · María S. López-Gutiérrez

Received: 17 May 2013 / Accepted: 4 October 2013 / Published online: 15 October 2013
© Springer Science+Business Media New York 2013

Abstract The aim of this work was to investigate the aqueous mercury adsorption in a fixed bed of mesostructured silica SBA-15 functionalized with propylthiol by co-condensation (SBA-15-SH). Powdered synthesized adsorbents were used to prepare pellets with sizes ranging from 0.5 to 1 mm. The physicochemical properties determined from N_2 adsorption and chemical analysis were compared for powder and pellets. Batch static experiments were carried out to obtain the equilibrium mercury adsorption isotherms, resulting that although the maximum adsorption capacity was reduced from powder to pellets, the materials maintained high efficiency for mercury removal even at very low aqueous metal concentration. Dynamic experiments were carried out in a fixed bed column by modifying the volumetric flow rate, bed length, inlet concentration, and amount of propylthiol groups incorporated to the adsorbent, and analyzing the temporal scale and the mercury adsorption capacities. The elution of the fixed bed was carried out chemically by circulating an aqueous 2 M hydrobromic acid stream for 2 h so achieving a complete recovery of the mercury previously adsorbed. Simplified dynamic equations of Bohart–Adams and Wolborska were used for modeling the breakthrough curves.

J. M. Arsuaga · A. Arencibia (✉)
Department of Chemical and Energy Technology, ESCET, Rey Juan Carlos University, C/Tulipán, s/n, 28933 Móstoles, Madrid, Spain
e-mail: amaya.arencibia@urjc.es

J. Aguado · M. S. López-Gutiérrez
Department of Chemical and Environmental Technology, ESCET, Rey Juan Carlos University, C/Tulipán, s/n, 28933 Móstoles, Madrid, Spain

Keywords Aqueous mercury adsorption · Heavy metal removal · Propylthiol functionalized materials · Fixed bed adsorption · Mesostructured materials

1 Introduction

Mercury is one of the most toxic heavy metals found in the environment being mainly deposited in water by anthropogenic and natural sources as Hg(II) (UNEP 2013). Due to its bioaccumulative properties and non-degradability, it is extremely hazardous even in small quantities and hence, worldwide governments have adopted very restrictive limits for mercury concentration in water. For drinking water, standard values of 1 and 2 μg L^{-1} were adopted by EU (EC Regulation 2007) and USEPA (EPA 2009).

Adsorption is a valuable technique for aqueous mercury removal due to its operation simplicity without using chemical reactants, easiness for waste treatment and the availability of a wide range of adsorbents. Mesostructured silica materials functionalized with organic sulfur have received special attention as aqueous mercury sorbents since they are highly efficient at low and very low concentrations and exhibit important adsorption capacities (Walcarius and Mercier 2010). Many researchers have reported studies concerning the synthesis based on the wide variety of mesostructured solids (MCM, HMS, MSU, SBA) (Feng et al. 1997; Mercier and Pinnavaia 1997; Aguado et al. 2005; Antochshuk et al. 2003). The main features of these adsorbents are the presence of thio-derivatives as active adsorption sites with high affinity for mercury, as well as their high pore volume and narrow pore size distribution which allows for the easy diffusion of mercury species to the sulfur groups.

Our group has developed efficient adsorbents based on the functionalization of SBA-15 mesostructure with propylthiol groups by co-condensation of tetraethoxysilane (TEOS) and 3-mercaptopropyltrimethoxysilane (MPTMS). The resulting SBA-15-SH adsorbents incorporate a large amount of thiol groups completely accessible to mercury species as they present suitable textural and structural properties achieving adsorption capacities as high as 4.2 mmol of mercury per gram (Aguado et al. 2005, 2008). It has been well established that high loadings of propylthiol groups can be incorporated in the adsorbent maintaining good accessibility to all of them because the mesoscopic order of the parent structure is preserved.

There are few investigation reported in the literature about heavy metal removal from water by adsorption in fixed bed column using organic functionalized mesostructured materials. A short study was firstly described for cation-exchange chromatographic application of SBA-15 modified with carboxylic groups (Bruzzoniti et al. 2007). Also, the performance of SBA-15 silica functionalized with melanine-based dendrimer amines in a fixed bed column was investigated as adsorbent of Pb(II), Cu(II), and Cd(II) (Shahbazi et al. 2011). More recently, Da'na and Sayari (2013) reported the dynamic adsorption of copper ions in a packed bed of aminopropyl modified SBA-15 pellets. To our knowledge, there are no studies focused on the elimination of mercury by functionalized mesostructured silica in fixed bed column.

In the present work, the behavior of thiol functionalized SBA-15 material working in a small scale fixed bed was studied. In order to explore the possibility of using these mercury adsorbents in a fixed bed, materials were pelletized under pressure and characterized in comparison with the powder form. Column adsorption process was analyzed by modifying the flow rate, inlet adsorbate concentration, and thiol amount in adsorbent as operating conditions. Two simplified models have been applied to reproduce the dynamic column adsorption.

2 Materials and methods

2.1 Reagents

Tetraethoxysilane [$(CH_3CH_2O)_4Si$], MPTMS [$(CH_3O)_3Si(CH_2)_3SH$] and surfactant Pluronic P123 [triblock poly(ethylene oxide)-poly(propylene oxide)-poly(ethylene oxide), ($PEO_{20}PPO_{70}PEO_{20}$)], were used as silica and organic precursors and structure directing agent, respectively. All chemicals were purchased from Aldrich and used as received. For adsorption experiments, mercury chloride ($HgCl_2$, synthesis grade) from Fluka was chosen while mercury standard solution supplied by Fluka as 1.0 g/L mercuric nitrate in 0.1 mol/L HNO_3 medium was used as standard for analysis.

2.2 Adsorbent synthesis

Propylthiol-functionalized mesoporous SBA-15 silica obtained by co-condensation was prepared according to the procedure previously published (Aguado et al. 2005). 4 g of Pluronic P123 were dissolved at room temperature in 125 mL of 1.9 mol/L HCl, and heated up to 40 °C. TEOS (37 mmol) was added to the solution that was stirred for 45 min before adding the amount of MPTMS organosilane precursor needed to obtain a MPTMS/TEOS molar ratio of 0.1 or 0.4 in the synthesis medium. The stirring was maintained for 20 h and aged for 24 h at 100 °C. Solid material was recovered by filtration and then dried. The template was extracted with ethanol under reflux for 24 h and the remaining solid product was filtered and dried at 100 °C for 2 h. These adsorbent materials were denoted as SBA-15-SH-10 and SBA-15-SH-40.

Since freshly prepared materials are pulverulent with very small particle size (around 1 μm), a large pressure drop in the fixed bed is observed when using in this form. Therefore, pellets of SBA-15-SH adsorbents were prepared by means of a matrix placed within a hydraulic press working at 1,800 kg cm^{-2} during 90 s. The pellets were subsequently broken and sieved through two meshes with 1 mm and 0.5 mm to get an intermediate size.

2.3 Characterization of synthesized adsorbents

Nitrogen adsorption–desorption isotherm at 77 K were acquired using a Tristar 3000 Micromeritics equipment. Samples were outgassed in N_2 flow for 8 h at 150 °C before analysis. Linearized B.E.T. equation was applied in the range of relative pressures from 0.05 to 0.20 to determine the BET surface area and pore size distributions were obtained using the B.J.H. model from the adsorption branch of the isotherm (assuming cylindrical pore geometry). Total pore volume was calculated at a relative pressure around 0.97 (Sing et al. 1985). Organic sulfur content was determined by elemental analysis in a Vario EL III Elementar Analyzer System GMHB.

2.4 Mercury adsorption batch experiments

Batch experiments were conducted to obtain the experimental adsorption isotherms of Hg(II) from aqueous solution corresponding to powder and pellet forms of materials. Single runs were carried out by stirring 25 mg of adsorbent in 45 mL of aqueous metal solution at 20 °C during equilibrium time, previously determined as 3 h for powder form. Mixtures were filtered with a syringe filter of

0.22 μm and the final solutions were collected. To obtain the isotherm corresponding to pellets, the equilibration was maintained for 24 h without stirring to avoid further fragmentation.

Initial and equilibrium Hg(II) concentrations were determined by cold vapour atomic fluorescence spectroscopy (CV-AFS) with an Analytical Milleniun Merlin spectrometer after calibration with stock solutions according to the EN 13506 standard procedure (AENOR 2002). For mercury concentration higher than 0.1 mg L^{-1}, the analysis was carried out by inductive coupled plasma-atomic emission spectroscopy in a Varian Vista AX (ICP-AES) following the standard EPA method 200.7 (EPA 2001). Adsorbed mercury amount was calculated by difference between initial and final metal concentrations in the solution.

2.5 Fixed bed column adsorption experiments

Continuous flow experiments were conducted in a fixed bed using borosilicate glass column with a length of 15 cm and an internal diameter of 4 mm. The column was packed with the SBA-15-SH-*x* material placed between two small layers (2 mm) of glass wool using two bed heights. The aqueous mercury solution was passed through the vertical column flowing by gravity from an upper tank; solution flow rate was regulated by means of a control valve. The effluent solution was collected at selected time intervals, and the Hg(II) concentration was determined by CV-AFS (AENOR 2002). Prior to the experiments with mercury solutions, fixed bed was conditioned by Milli-Q water circulation for 4 h.

All experiments were performed at 20 °C and natural pH of mercury aqueous solution (~4.5). $HgCl_2$ solutions with metal concentration within 10–100 mg L^{-1} and volumetric flow rates varying from 10 to 160 mL/h were tested for two different bed height, 5 cm and 10 cm, corresponding to 0.35 g and 0.7 g of adsorbent, respectively.

Fixed bed column performance is usually evaluated using the breakthrough curves obtained by plotting the dimensionless concentration C_t/C_0 versus time or volume of the effluent, where C_t and C_0 are the outlet and inlet adsorbate concentration, respectively (Cooney 1999). The breakthrough time, t_b, was determined when the Hg(II) concentration in the effluent reached 2 % of the influent value. The saturation time, often called exhaustion time, t_e, was estimated when mercury concentration achieved 95 % value of the influent.

Total Hg(II) adsorbed, q_{total} (mg), in the column for a specific flow rate and initial concentration was calculated from following equation:

$$q_{total} = \frac{QC_0}{1000}\int_{t=0}^{t=t_{total}}\left(1-\frac{C}{C_0}\right)dt \quad (1)$$

where Q is the flow rate. The total amount of Hg(II) that pass through the column, m_{total} (mg), and the removal percentage was calculated according to Eq. 2 and 3, respectively.

$$m_{total} = \frac{C_0 Q t_e}{1000} \quad (2)$$

$$R = \frac{q_{total}}{m_{total}} \times 100 \quad (3)$$

On the other hand, the mass transfer zone (MTZ) used to estimate the bed region where most of the adsorption occurs was determined for every experiment as:

$$\mathrm{MTZ} = L\frac{t_e - t_b}{t_e} \quad (4)$$

where L is the bed height.

2.6 Breakthrough modeling

In this work two simplified models with analytical solutions (Bohart–Adams and Wolborska) were applied to reproduce the mercury adsorption dynamics in the fixed bed column.

The Bohart–Adams model is one of the most frequently used to predict the breakthrough curve in adsorption columns (Bohart and Adams 1920). In this model, the intraparticle diffusion and external resistance for mass transfer are neglected and the adsorption kinetics is controlled by the surface chemical reaction between adsorbent and sorbate. Additionally, it is assumed that: (i) axial and radial dispersions are absent in the fixed bed column; (ii) column void fraction remains constant; (iii) physical properties of solid and fluid phases are invariant.

The mass balance differential equation for a fixed bed column is given by:

$$\frac{\partial C}{\partial t} + v\frac{\partial C}{\partial x} + \frac{(1-\varepsilon)}{\varepsilon}\frac{\partial q}{\partial t} = D\frac{\partial^2 C}{\partial x^2} \quad (5)$$

where C is the adsorbate fluid concentration, q is the adsorbed amount, v the interstitial speed, ε is the void fraction, D is the axial diffusion coefficient, and x and t are the axial coordinate and time. The analytical solution of the model is obtained for a rectangular adsorption isotherm yielding the following equation:

$$\frac{C}{C_0} = \frac{e^{t'}}{e^{x'} + e^{t'} - 1} \quad (6)$$

where $t' = k_{BA}C_0 t$ and $x' = \frac{k_{BA}q_0 L}{v}\left(\frac{1-\varepsilon}{\varepsilon}\right)$.

L and C_0 are the column length and the inlet solution concentration. k_{BA} is the Bohart–Adams rate constant, and q_0 the maximum sorption capacity per unit mass. Eq. 6 can be converted to the simplified linear form:

$$\ln\left(\frac{C_0}{C}-1\right)=\frac{k_{BA}N_0L}{U}-k_{BA}C_0t \quad (7)$$

where N_0 is defined as the sorption capacity per unit volume of the bed and U is the superficial velocity of the fluid.

The Bohart–Adams model can be considered as a simplified form of the more general Thomas model (Thomas 1944). When the equilibrium adsorption isotherm is highly favorable, the Thomas and Bohart–Adams models approach (Borba et al. 2008; Chu 2010; Hashim and Chu 2007) and, with the suitable approximations, lead to the same integrated linear equation that is commonly used to design columns for wastewater treatment (Cooney 1999). It is worth to mention here that many reports in the recent literature regarding environmental adsorption and biosorption make use of an analytical lineal expression similar to Eq. 7, but confusing denoted as Thomas model (Chu 2010).

The Wolborska model was derived from the general equations of mass transfer in the range of relative low concentration of the breakthrough curve, which is controlled by the external mass transfer from the solution to the adsorbent surface and by the axial diffusion (Wolborska 1989). The linear analytical solution is expressed by Eq. 8 in terms of the kinetic coefficient of external mass transfer, β_a, that includes the effect of both axial dispersion and external mass transfer.

$$\ln\left(\frac{C}{C_0}\right)=\frac{\beta_a C_0}{N_0}t-\frac{\beta_a}{U}L \quad (8)$$

where the kinetic coefficient of the external mass transfer is given by:

$$\beta_a=\frac{U_0}{2D}\left(\sqrt{1+\frac{4\beta_0 D}{U^2}}-1\right) \quad (9)$$

β_0 represents the external mass transfer coefficient with a negligible axial dispersion; the meaning of D, U, and N_0 is as previously mentioned.

3 Results and discussion

3.1 Physicochemical characterization of powder and pellets SBA-15-SH adsorbents

Thiol-functionalized SBA-15 materials containing 10 and 40 % of organic precursor were prepared in this work by co-condensation and subsequently pelletized and sieved. The whole physical and chemical characterization of the adsorbents SBA-15-SH-x in powder form was previously reported (Aguado et al. 2008) and a brief summary of their textural properties and sulfur content is recorded here just for comparison with the novel characterization of the pelletized materials. As seen in Fig. 1, the nitrogen adsorption–desorption isotherms at 77 K belong to IV IUPAC type (Sing et al. 1985) indicating the mesoporous nature of these materials. Adsorbed nitrogen volume is clearly higher for the sample functionalized with less organic amount and for pulverulent materials reflecting more porous structures in these cases.

Pore size distribution calculated for SBA-15-SH-10 powder exhibits a narrow peak indicating a homogeneous mean pore size. Wider pore size distributions were found both for SBA-15-SH-40 powder and pelletized materials due to an irregular size of pores caused either by the interference of thiol groups or by pore collapse as consequence of the external applied pressure.

Table 1 summarizes the relevant textural properties (pore diameter, D_p, BET surface area, S_{BET}, and pore volume, V_p) of the SBA-15-SH-x adsorbents along with the sulfur content. Textural parameters strongly reduce when organic functionalization increases showing changes in the BET surface area from 680 to 146 $m^2\ g^{-1}$ and pore volume from 0.79 to 0.19 $cm^3\ g^{-1}$ corresponding to roughly 80 % of modification. In addition, the pelletization process results in a significant diminution of textural properties due to compaction and partial collapse of the internal structure because of applied pressure. Thus, pore volume of SBA-15-SH-10 samples diminishes from 0.79 to 0.47 $cm^3\ g^{-1}$ when pellets are formed what represents a 40 % change. The reduction is even higher for SBA-15-SH-40, around 50 %. Mean pore diameter also decreased and a significant reduction of surface area was observed as well due to mechanical compression, but the mesoporous properties were usually preserved. On the other hand, the sulfur content of the samples, 1.2 mmol S g^{-1} (SBA-15-SH-10) and 3.7 mmol S g^{-1} (SBA-15-SH-40) exhibited no difference between powder and pellets forms.

3.2 Mercury equilibrium isotherms

Mercury adsorption isotherms were obtained at 20 °C by means of batch experiments where the initial mercury concentration varied from 30 to 450 mg L^{-1}. Figure 2 displays the experimental Hg(II) isotherms plotted as the amount of mercury adsorbed at equilibrium, q_e (milimole per gram of adsorbent) as a function of the equilibrium mercury concentration in the liquid phase, C_e (mg L^{-1}). As it has been already explained (Aguado et al. 2005, 2008), the isotherms are Langmuir type or L2-type according to Giles' classification (Giles 1974), with sharp initial slopes, so indicating that materials act as highly effective adsorbents at very low concentration, and apparent saturation values at higher Hg(II) concentration. The maximum

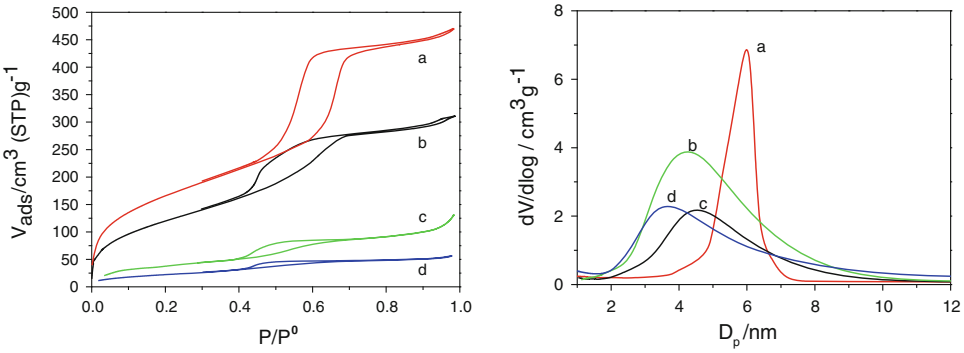

Fig. 1 Nitrogen adsorption–desorption isotherms at 77 K (*left*) and B.J.H. pore size distributions measured for powder and pellet solids (*right*). (*a*) Powder SBA-15-SH-10, (*b*) pellets SBA-15-SH-10, (*c*) powder SBA-15-SH-40, and (*d*) pellets SBA-15-SH-40

Table 1 Textural parameters, sulfur content, and Hg(II) adsorption capacity estimated for SBA-15-SH adsorbents in powder and pellets

Adsorbent	D_p (nm)	S_{BET} (m^2 g^{-1})	V_p (cm^3 g^{-1})	Sulfur content (mmol S g^{-1})	Q_o (mmol Hg g^{-1})
SBA-15-SH10 powder	6.2	680	0.79	1.2	1.20
SBA-15-SH10 pellets	4.6	416	0.47	1.2	0.87
SBA-15-SH40 powder	4.4	145	0.19	3.71	3.60
SBA-15-SH40 pellets	3.6	83	0.084	3.71	–

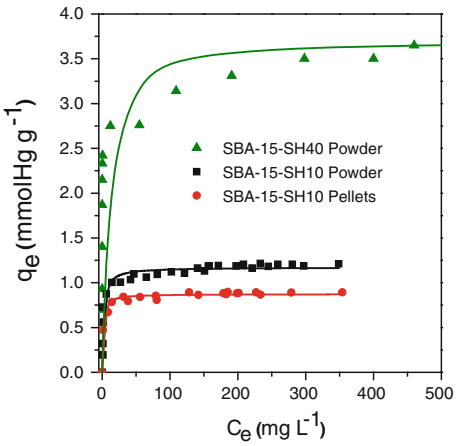

Fig. 2 Aqueous mercury adsorption isotherms determined at 20 °C for powder and pellets SBA-15-SH adsorbents. Curves correspond to the Langmuir isotherm estimated from linear fitting

adsorption mercury loading Q_0 was calculated from the linearized Langmuir equation:

$$C_e/q_e = 1/Q_0 b + C_e/Q_0 \quad (10)$$

where Q_0 y b are the characteristic Langmuir parameters related to the maximum adsorption capacity and intensity of adsorption, respectively.

As displayed in Table 1, the maximum adsorption capacity of SBA-15-SH-10 and SBA-15-SH-40 in powder form fairly matches the sulfur content proving that mercury species fully reach all the active sites with a 1:1 mercury-sulfur bonding, thus providing adsorption capacities as high as 3.6 mmol Hg(II) g^{-1}. It is worth to mention here that in our experimental conditions maximum adsorption uptake are achieved for Hg(II) aqueous initial concentration higher than 400 mg L^{-1}. However, these materials are also very efficient at low concentration since mercury levels lower than 300 mg L^{-1} can be easily reduced below 1 mg L^{-1} using the SBA-15-SH-40 adsorbent. Solutions with smaller concentrations, more frequent in wastewater, can be treated by any of the adsorbents to achieve values close to 1 μg L^{-1}.

Prior to the study of adsorption process in the fixed bed column, the isotherm of aqueous Hg(II) adsorption corresponding to SBA-15-SH-10 in pellets form was obtained and compared with the experimental isotherm for the powder form. As seen in Fig. 2, the process of pellets formation clearly affects the mercury adsorption capacity since the Q_0 value decreases from 1.20 to 0.87 mmol Hg g^{-1} because a fraction of thiol groups anchored to the silica surface turns inaccessible by pore collapse. However, this diminution of around 27 % is only relevant at saturation corresponding to high mercury concentrations not usually found in wastewater. At low and very low mercury concentration both forms of SBA-15-SH adsorbent are extremely efficient as shows the highly pronounced slope of the isotherms.

3.3 Breakthrough curves for mercury adsorption

Adsorption dynamic tests were conducted in a fixed bed column in order to obtain the breakthrough curves for mercury removal. SBA-15-SH-10 material was chosen as adsorbent for most experiments because this sample preserves suitable textural properties and adequate adsorption

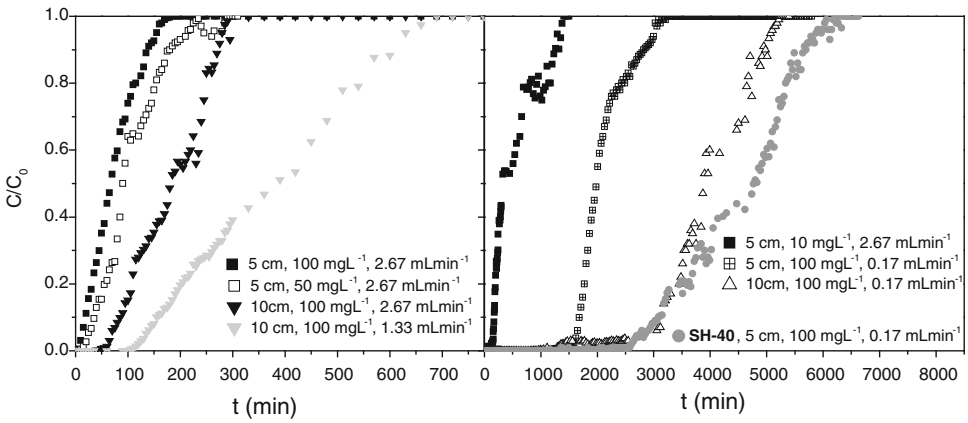

Fig. 3 Experimental breakthrough curves for Hg(II) adsorption on SBA-15-SH-10 and SBA-15-SH-40

Table 2 Dynamic parameters calculated from the experimental breakthrough curves

Adsorbent	C_o (mg L^{-1})	L (cm)	Q (mL min^{-1})	t_b 2 % (min)	t_e 95 % (min)	q_{total} (mg)	q_b (mg)	Removal (%)	MTZ (cm)
SH-10	100	10	0.17	1380	5070	66	23	79	6.5
SH-10	100	10	1.33	120	630	50	15	59	6.9
SH-10	100	10	2.67	65	280	49	17	65	6.5
SH-10	100	5	0.17	1560	3000	35	26	70	1.3
SH-10	100	5	2.67	10	155	20	2.6	47	4.3
SH-10	50	5	2.67	20	215	14	2.6	50	4.1
SH-10	10	5	2.67	130	1320	14	3.4	42	3.8
SH-40	100	5	0.17	2610	5880	75	34	77	2.7

capacity. SBA-15-SH-40 material was occasionally used for comparison in selected conditions.

3.3.1 Influence of the operating conditions

Column studies were conducted by modifying the flow rate from 0.17 to 2.67 mL min^{-1}, the column length ($L = 5$ cm and $L = 10$ cm), and the initial concentration from 10 to 100 mg L^{-1}. Fig. 3 shows the experimental breakthrough curves and Table 2 lists the parameters extracted from the kinetic profiles.

At high flow rates, steep breakthrough curves were found with early breakthrough (10 min–2 h) and exhaustion times; conversely, at low flow rate, much larger times were obtained for both breakthrough (at least 23 h) and also exhaustion. In addition, asymmetric curves were found with smaller slopes. The asymmetry of the curves could indicate that multiple resistances can simultaneously be controlling the process, i.e., external or internal diffusion through different types of pores (micro, meso and macro) and along the surface.

As seen in the Table 2 the adsorption capacity is significantly higher when the flow rate is low. For the lowest value, the total Hg(II) uptake yields a notable removal percentage of 78.5 %, what means that effective adsorption took place along the column, so indicating that the thiol adsorption sites are available to capture Hg(II) species around or inside the pelletized adsorbent. When flow rate rises the removal percentage reduces to nearly 60 %, since the external film resistance tends to decrease along with the residence time and shorter rupture times are produced because many mercury species pass through the column with insufficient time to enter the mesoporous structure of the particles and lower adsorption capacities are obtained.

The amount of Hg(II) adsorbed at breakthrough was thoroughly smaller than the values corresponding to the exhaustion point due to the broad mass transfer zone (MZT) related to the bed length; thus, the estimated MTZ values were higher than 65 % of the column height. The differences between the amount adsorbed in the rupture and the exhaustion points were more important for high flow rates. Besides, when $L = 10$ cm, MTZ was almost independent of the flow rate ($\sim$6.5 cm), while for $L = 5$ cm there was a large dispersion from 1.3 to 4.3 cm.

On the other hand, the Hg(II) adsorption capacity per unit mass was found to be independent of the bed length. As an example, for experiments carried out with 100 mg L^{-1} and 0.17 mL min^{-1}, mercury uptakes for $L = 10$ cm and $L = 5$ cm were 66 mg and 35 mg, respectively (Table 2). Taking into account the mass used for filling the column bed (0.70 and 0.35 g), the values calculated for Hg(II) adsorption capacity were 95 mg g^{-1} ($L = 10$ cm) and 100 mg g^{-1}

($L = 5$ cm) or 0.47 and 0.5 mmol Hg g^{-1}, respectively, thus indicating that the adsorption capacity is proportional to the adsorbent amount. Although these dynamic values of mercury uptake are lower than the ones obtained in static batch experiments (around 30 %), it must be emphasize that the SBA-15-SH materials maintain high adsorption capacities in the fixed bed.

As seen in the Table 2, the increase of feed mercury concentration from 10 to 100 mg L^{-1} yielded an apparent shortening on the breakthrough and exhaustion times since the accessible thiol groups are more quickly saturated due to the elevated driving force. At low initial concentration, breakthrough time delays and the slope of curve decreases pointing to a slower mass transfer.

The analysis of the dynamics corresponding to the SBA-15-SH-40 sample compared with SBA-15-SH-10 showed that the slope found for the breakthrough of SBA-15-SH-40 material is notably lower. This behavior was ascribed to a much slower mass transfer due to diffusion resistance as a consequence of the poorer textural properties of the SBA-15-SH-40 pellets. Moreover, the Hg(II) adsorbed amount estimated for the breakthrough point (26 mg and 34 mg for the SBA-15-SH-10 and SBA-15-SH-40, respectively) confirmed that the number of active sites available for easy adsorption was just slightly higher for SBA-15-SH-40 pellets although the loading of thiol groups of the material is much higher.

On the other hand, the mercury total uptake determined for SBA-15-SH-40 was 215 mg g^{-1} (1.07 mmol g^{-1}), being the double than the value calculated for SBA-15-SH-10 (0.5 mmol g^{-1}). The comparison with the equilibrium isotherms showed that the maximum adsorption capacity was 3 times higher for SBA-15-SH-40 than for SBA-15-SH-10 for materials in powder form. This result demonstrated that there are multiple thiol groups in the SBA-15-SH-40 adsorbent that remain uncovered by Hg(II) species since the accessibility is more restrictive as a result of the appreciable diminution detected for pore size, surface area, and pore volume after pelletization.

Taking into account the obtained results it can be extracted that the best results in terms of mercury adsorption capacity was obtained at low volumetric flow; however, very long experimental times are needed and hence, practical application would be difficult. Nevertheless, it is worth to mention that a significant adsorption capacity could be obtained regardless the reduction of textural properties. Therefore, an extended study on the pelletization process to reduce mass transfer problems will clarify the potential use of these adsorbents in dynamic fixed bed columns.

3.3.2 *Breakthrough modeling*

The dynamic behavior of the fixed bed column was modeled through the two above mentioned models (Bohart–Adams and Wolborska) using the linearized forms, Eq. 7 and 8, respectively. Two fits to the experimental profiles were tested for each model, one fit up to breakthrough point, t_b, and another fit up to exhaustion time, t_e. Table 3 summarizes the relevant estimated kinetic parameters as well as the regression coefficients. Fig. 4 illustrates the comparison between experimental and estimated values.

Most of Bohart–Adams fits up to rupture point yielded poor regression coefficients lower than 0.7, while fits for the whole curve was much better (R^2 values near 1). Consequently, for this model the whole predicted curve was used to compare with experimental data. As seen in the figure, the modeled curves roughly fit the overall profile, although without reproducing any asymmetry of the experimental curve. The values recorded in Table 3 for the kinetic coefficients k_{AB} strongly enlarged when volumetric flow rate and inlet concentration increased. In contrast, k_{BA} decreased for the longer bed height and the highly loaded adsorbent. For example, the change from $L = 5$ cm to $L = 10$ cm for $C_0 = 100$ mg L^{-1} and $Q = 0.17$ mL min^{-1} yielded k_{AB} values of 5.3·and 1.9 × 10^{-5} L mg^{-1} min^{-1}, respectively, while the Bohart–Adams constant for same conditions was

Table 3 Estimated parameters extracted from the fitting using the Bohart–Adams and Wolborska model

Experimental conditions				Bohart–Adams		Wolborska	
Adsorbent	C_o (mg L^{-1})	L (cm)	Q (mL min^{-1})	10^5 k_{BA} (L mg^{-1} min^{-1})	R^2	β (min^{-1})	R^2
SH-10	100	10	0.17	1.9	0.95	1.60	0.94
SH-10	100	10	1.33	14.7	0.66	16.4	0.61
SH-10	100	10	2.67	31.3	0.80	29.2	0.94
SH-10	100	5	0.17	5.3	0.93	3.90	0.91
SH-10	100	5	2.67	39.5	0.91	30.6	0.99
SH-10	50	5	2.67	70.8	0.85	40.6	0.91
SH-10	10	5	2.67	58.0	0.67	33.3	0.75
SH-40	100	5	0.17	2.5	0.83	1.40	0.58

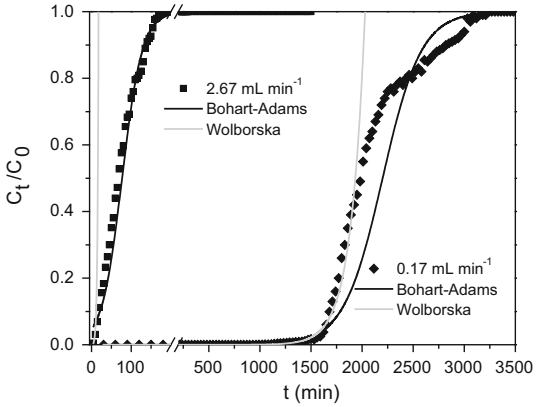

Fig. 4 Comparison between experimental and calculated breakthrough curves for Bohart–Adams and Wolborska models ($L = 5$ cm, $C_0 = 100$ mg L^{-1})

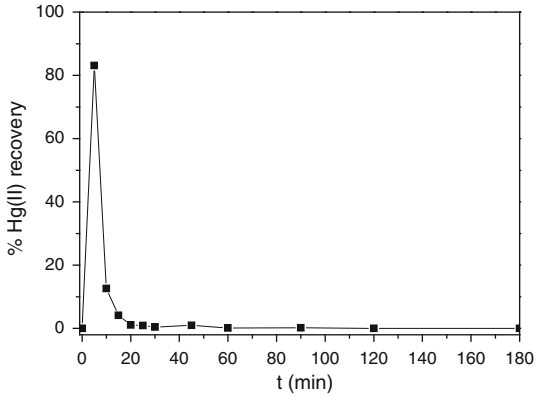

Fig. 5 Percentage of mercury recovery as a function of time by using a 2 M aqueous solution of HBr. $L = 5$ cm, $Q = 0.17$ mL min^{-1}, $C_0 = 50$ mg L^{-1}

estimated as 2.5×10^{-5} L mg^{-1} min^{-1} for the SBA-15-SH-40. These values are comparable with the scarcely previous reported values corresponding to the adsorption of rather similar aqueous metals (Cu, Pb, and Cd) on mesoporous silica materials, but functionalized with dendrimer amines (Shahbazi et al. 2011).

Wolborska model was also tested up to rupture and exhaustion points, but the regression coefficients showed that fits were only adequate until the breakthrough time. Table 3 summarizes the Wolborska fitting to the initial breakthrough curve. As seen, R^2 values were frequently found higher than 0.9. The success of this model is clear at the beginning (Fig. 4), since the predicted values exactly match the initial part of the curve, so the estimation of the breakthrough time should be correct. Fig. 4 also illustrates that the Wolborska model completely fails in the prediction of the second part of the experimental profiles. As seen in Table 3 the influence of operation conditions on the β parameter is analogous to the variation found for the Bohart–Adams kinetic coefficients. In general, since the two models reproduced satisfactorily the initial part of the curves, that is the most relevant section as determining the useful capacity of the fixed bed column, they could give a good idea about the fixed column efficiency although it should be taken into account that the application should be done from an empirical point of view.

3.3.3 Column elution

The elution of mercury loaded within the fixed bed columns was investigated by using an aqueous solution of HBr. This compound was selected as chemical agent for regeneration of thiol groups due to the cooperative effect of acidic medium and mercury complexation ability of bromide (Arencibia et al. 2010). Experiments were carried out after mercury loading with the operational set $L = 5$ cm, $C_0 = 10$ mg L^{-1} and $Q = 2.67$ mL min^{-1}. An aqueous HBr solution (2 M) was passed through the column during 3 h and the mercury recovery percentage was monitored versus time. As seen in Fig. 5 that displays the obtained results, a significant recovery of Hg(II), higher than 80 % was immediately detected, achieving 99.8 % of recovery after 1 h.

4 Conclusions

This work demonstrated that thiol-functionalized SBA-15 materials could be used as effective adsorbent for mercury removal in a fixed bed column of pelletized samples. After pellets formation, the amount of thiol groups has been found similar, but textural properties of adsorbents diminished. Thus, although a reduction in maximum adsorption capacity of the equilibrium isotherms was observed through static experiments, the efficiency of materials at low aqueous mercury concentration was preserved. The influence of volumetric flow rate, bed length, inlet concentration, and amount of propylthiol groups incorporated to the adsorbent was evaluated in dynamic experiments with a fixed bed column. The analysis of the breakthrough curves showed that significant mercury removal can be achieved at low flow rates and for materials with high propylthiol groups content, although large time consuming was required. The elution of mercury species loaded on the adsorbents was successfully reached by circulating an aqueous 2 M hydrobromic acid stream for 2 h. Simplified kinetic equations of Bohart–Adams and Wolborska were suitable to reproduce the first section of the experimental breakthrough curve, but Wolborska fit is superior; conversely, Bohart–Adams predictions were adequate to qualitatively mimic the whole curve until the exhaustion time.

Acknowledgments This work has been supported by the Spanish Government through the project CTM2009-08649 and CTM2012-34988. Regional Government of Madrid also financed this research through the Project "REMTAVARES" S-2009/AMB/1588.

References

AENOR: Calidad del agua. Determinación del mercurio por espectrometría de fluorescencia atómica. UNE-EN-13506 (2002)

Aguado, J., Arsuaga, J.M., Arencibia, A.: Adsorption of aqueous mercury (II) on propylthiolfunctionalized mesoporous silica obtained by cocondensation. Ind. Eng. Chem. Res. **44**, 3665–3671 (2005)

Aguado, J., Arsuaga, J.M., Arencibia, A.: Influence of synthesis conditions on mercury adsorption capacity of propylthiol functionalized SBA-15 obtained by co-condensation. Microporous Mesoporous Mater. **109**, 513–524 (2008)

Arencibia, A., Aguado, J., Arsuaga, J.M.: Regeneration of thiol-functionalized mesostructured silica adsorbents of mercury. Appl. Surf. Sci. **256**, 5453–5457 (2010)

Antochshuk, V., Olkhovyk, M., Jaroniec, I., Park, S.M., Ryoo, R.: Benzoylthiourea-modified mesoporous silica for mercury(II) removal. Lagmuir **19**(7), 3031–3034 (2003)

Bohart, G.S., Adams, E.Q.: Some aspects of the behavior of charcoal with respect to chlorine. J. Am. Chem. Soc. **42**, 523–544 (1920)

Borba, C.S., Da Silva, E.A., Fagundes-Klen, M.R., Kroumov, A.D., Guirardello, R.: Prediction of the copper (II) ions dynamic removal from a medium by using mathematical models with analytical solution. J. Hazard. Mater. **152**, 366–372 (2008)

Bruzzoniti, M.C., Prelle, A., Sarzanini, C., Onida, B., Fiorilli, S., Garrone, E.: Retention of heavy metal ions on SBA-15 mesoporous silica functionalised with carboxylic groups. J. Sep. Sci. **30**, 2414–2420 (2007)

Chu, K.H.: Fixed bed sorption: setting the record straight on the Bohart–Adams and Thomas models. J. Hazard. Mater. **177**, 1006–1012 (2010)

Cooney, D.O.: Adsorption Design for Wastewater Treatment. Lewis Publishers, Boca Raton (1999)

Da'na, E., Sayari, A.: Adsorption of copper on amine-functionalized SBA-15: predicting breakthrough curves. Environ. Eng. **139**(1), 95–103 (2013)

Environment, Community and Local Government: European Communities (Drinking Water) Regulations. Statutory Instruments. S.I. No. 106 (2007)

EPA: Method 200.7. Trace Elements in Water, Solids and Biosolids by Inductively Coupled Plasma-Atomic Emission Spectroscopy. EPA-821-R-021-01-010 (2001)

EPA: List of Contaminants and their MCLs. EPA 816-F-09-0004 (2009)

Feng, X., Fryxell, G.E., Wang, Q., Kim, A.Y., Kemmer, K.M.: Functionalized monolayers on ordered mesoporous supports. Science **233**, 923–926 (1997)

Giles, C.H., D′Silva, A.P., Easton, I.A.: A general treatment and classification of the solute adsorption isotherm II. Experimental interpretation. J. Colloid Interface Sci. **47**(3), 66–777 (1974)

Hashim, M.A., Chu, K.H.: Prediction of protein breakthrough behavior using simplified analytical solutions. Sep. Purif. Technol. **53**, 189–197 (2007)

Mercier, L., Pinnavaia, T.J.: Accces in mesoporous materials: advantages of a uniform pore structure in the design of a heavy metal ion adsorbent for environmental remediation. Adv. Mater. **9**, 500–503 (1997)

Shahbazi, A., Younesia, H., Badiei, A.: Functionalized SBA-15 mesoporous silica by melamine-based dendrimer amines for adsorptive characteristics of Pb(II), Cu(II) and Cd(II) heavy metal ions in batch and fixed bed column. Chem. Eng. J. **168**, 505–518 (2011)

Sing, K.S.W., Everett, D.H., Haul, R.A.W., Moscon, L., Pierotti, R.A., Rouquerol, J., Siemieniewska, T.: Reporting physisorption data for gas/solid systems with special reference to the determination of surface area and porosity. Pure Appl. Chem. **57**(4), 603–619 (1985)

Thomas, H.C.: Heterogeneous ion exchange in a flowing system. J. Am. Chem. Soc. **66**, 1664–1666 (1944)

UNEP: Global Mercury Assessment 2013, Sources, Emissions, Releases and Environmental Transport. UNEP Chemicals Branch, Geneva (2013)

Walcarius, A., Mercier, L.: Mesoporous organosilica adsorbents: nanoengineered materials for removal of organic and inorganic pollutants. J. Mater. Chem. **20**, 4478–4511 (2010)

Wolborska, A.: Adsorption on activated carbon of p-nitrophenol from aqueous solution. Wat. Res. **23**(1), 85–91 (1989)